Properties of Core−Shell Ni−Au Nanoparticles Synthesized through a Redox-Transmetalation Method in Reverse Microemulsion

Dong Chen,[†] Jiajun Li,[†] Chunsheng Shi,*[,†] Xiwen Du,[†] Naiqin Zhao,[†] Jing Sheng,[†] and Shuo Liu[‡]

School of Materials Science and Engineering and School of Chemical Engineering and Technology, Tianjin University, Tianjin 300072, China

Received January 19, 2007. Revised Manuscript Received April 29, 2007

Core−shell Ni−Au nanoparticles were chemically synthesized through a redox-transmetalation method in reverse microemulsion. The powder X-ray diffraction patterns revealed the presence of crystalline gold and nickel and the absence of any nickel oxides, nickel boride or other byproducts. The core−shell structure could be clearly observed by the transmission electron microscope. In addition, the Ni cores and the gold shells were further verified by the high-resolution transmission electron microscope and the Z-contrast image. The diameter of the nanoparticles ranged from 15 to 30 nm, with 5−10 nm core diameters and 5−10 nm shell thickness. The UV−visible absorption spectra of these nanoparticles showed a red shift (relative to pure gold nanoparticles), also in agreement with the gold shell morphology. For magnetic properties, the zero-field-cooled and field-cooled temperature dependence of the magnetization indicated the blocking temperature was at 16 K. The magnetization curves carried out at 5 K showed that the saturation magnetization, remanent magnetization, and coercivity at this temperature were 9.0 emu/g, 4.1 emu/g, and 2 kOe, respectively. The magnetization curves at 300 K presented the typical superparamagnetic behavior without any remains of remanent magnetization or coercivity, and the saturation magnetization at this temperature was 0.7 emu/g.

Introduction

In the past decades, considerable attention has been devoted to the preparation of magnetic nanoparticles because of their unique properties compared with corresponding bulk materials and the wide range of potential applications in optics, electronics, magnetic materials, catalytics, drug delivery systems, and so on.[1−4] Nanometer magnetic materials can exhibit superparamagnetic behavior, and the magnetic moment of superparamagnetic nanoparticles can reorient spontaneously because of thermal agitation in less than 1 ns.[5] Therefore, the superparamagnetic nanoparticles have become more and more important in many biomedical applications such as cell separation, biosensor technology, and magnetic resonance imaging.[6−8] The preparation of some magnetic metal nanoparticles such as iron, cobalt, and nickel is relatively more difficult because they are prone to be oxidation. For example, without proper protection, nickel nanoparticles are easily oxidized in the open air, so the usage of the nickel nanoparticles is seriously limited. Coating gold shells on the Ni nanoparticles can effectively relieve the oxidization process of the Ni cores and retain most of the favorable magnetic properties. Furthermore, the gold shell provides a platform for multifunctionalization, such as conjugation of biomolecules on account of the compatibility of gold with the human body.

A number of techniques have been used for the production of nanoparticles, such as gas-evaporation,[9] sputtering,[10] coprecipitation,[11] hydrothermal,[12] sol−gel method,[13] organic method,[14] microemulsion,[15] etc. One versatile method for synthesizing nanoparticles is the reverse water-in-oil microemulsion technique, which relies on the self-assembly nature of surfactants to push aqueous reactants into micelles.[16] Reverse water-in-oil microemulsions are transparent, isotropic liquid media with nanometer water droplets dispersed in a continuous oil phase and stabilized by surfactant molecules

* Corresponding author. Tel: 86-13332099162. Fax: 86-22-27891371. E-mail: csshi@tju.edu.cn.
[†] School of Materials Science and Engineering, Tianjin University.
[‡] School of Chemical Engineering and Technology, Tianjin University.

(1) Brieler, F. J.; Grundmann, P.; Froba, M.; Chen, L. M; Klar, P. J.; Heimbrodt, W.; Krug von Nidda H. A.; Kurz, T.; Loidl, A. *Chem. Mater.* **2005**, *17*, 795.
(2) Jiang, L. Q.; Gao, L. *Chem. Mater.* **2003**, *15*, 2848.
(3) Yi, D. K.; Lee, S. S.; Ying, J. Y. *Chem. Mater.* **2006**, *18*, 2459.
(4) Arruebo, M.; Galan, M.; Navascues, N.; Tellez, C.; Marquina, C.; Ibarra, M. R.; Santamaria, J. *Chem. Mater.* **2006**, *18*, 1911.
(5) Seymour, H. Koenig; Kenneth, E. Kellar. *Magn. Reson. Med.* **1995**, *34*, 227.
(6) Wang, D. S.; He, J. B.; Rosenzweig, N.; Rosenzweig, Z. *Nano Lett.* **2004**, *4*, 409.
(7) Chemla, Y. R.; Crossman, H. L.; Poon, Y.; McDermott, R.; Stevens, R.; Alper, M. D.; Clarke, J. *Proc. Natl. Acad. Sci. U.S.A.* **2000**, *97*, 14268.
(8) Ruehm, S. G.; Corot, C.; Vogt, P.; Kolb, S.; Debatin, J. F. *Circulation* **2001**, *103*, 415.
(9) Tanigaki, T.; Saito, Y.; Nakada, T.; Tsuda, N.; Kaito, C. *J. Nanopart. Res.* **2002**, *4*, 83.
(10) Babonneau, D.; Cabioc'h T.; Naudon, A.; Girard, J. C.; Denanot, M. F. *Surf. Sci.* **1998**, *409*, 358.
(11) Chen, Q.; Rondinone, A. J.; Chakoumakos, B. C.; Zhang, Z. J. *J. Magn. Magn. Mater.* **1999**, *194*, 1.
(12) Lu, Q. Y.; Gao, F.; Zhao, D. Y. *Nano Lett.* **2002**, *2*, 725.
(13) Chen, D. H.; He, X. R. *Mater. Res. Bull.* **2001**, *36*, 1369.
(14) Bao, Y. P.; Calderon, H.; Krishnan, M. K. *J. Phys. Chem. C* **2007**, *111*, 1941.
(15) Ji, M.; Chen, X. Y.; Wai, C. M.; Fulton, J. L. *J. Am. Chem. Soc.* **1999**, *121*, 2631.
(16) Hoener, C. F.; Allan, K. A.; Campion, A. J.; Fox, M. A.; Mallouk, T. E.; Weber, S. E.; White, J. M. *J. Phys. Chem. A* **1992**, *96*, 3812.

10.1021/cm070182x CCC: $37.00
Published on Web 06/12/2007

at the water−oil interface. These surfactant-covered water droplets offer a unique microenvironment for the formation of nanoparticles. With the dynamic nature of water droplets, aqueous components constrained in the water droplets can come together and react to form nanoparticles. The surfactants not only act as protective agents to inhibit the excess aggregation of nanoparticles but also restrict the growth of nanoparticles. The nanoparticles can be separated by organic phase and protected by the surfactants. So, the aggregation can be effectively restrained because they are difficult to approach. The size of the water droplet controlled by adjusting the molar ratio of water to surfactant can effectively constrain the growth of nanoparticles. As a result, the particles obtained in such a medium are generally quite uniform and monodispersed.[17]

The reverse microemulsion systems have been used to produce some metal and semiconductor nanoparticles such as Fe,[18] Ni,[19] Au,[20] ZnS, CdS,[21] Fe−Ni, and Cu−Ni alloy nanoparticles.[22,23] By adjusting the synthesis procedure, the method can even be applied to prepare the nanoparticles with a core−shell structure, such as core−shell Fe−Au and Fe−Silica nanoparticles,[24,25] and the diameter and thickness of core and shell can be well-controlled. Chen et al.[19,26] synthesized nickel nanoparticles in reverse microemulsion solutions using cationic surfactant. The mean diameter of the resultant nickel nanoparticles they obtained was round about 10 nm. The nanoparticles were not entirely superparamagnetic at 298.15 K; meanwhile, the feeble ferromagnetic behavior still remained. Legrand et al.[27] selected sodium borohydride and anion surfactant as the reducer and surfactant, respectively. What they obtained were not pure nickel nanoparticles but Ni_2B under nitrogen protection and a mixture of nickel and nickel boride in the open air. Cho et al.[24,28] synthesized core−shell Fe−Au nanoparticles, but they found the gold shells of the Fe−Au nanoparticles did not effectively protect the iron cores from oxidation. Carpenter and O'Connor et al.[29−31] also synthesized similar core−shell Fe−Au nanoparticles and other kinds of nanoparticles such as metallic cobalt, cobalt−platinum alloys, and gold-coated cobalt−platinum nanoparticles. In particular, the nanoparticles synthesized in reverse water droplet can be easily transferred into the aqueous phase. The property is of interest, because magnetic components contained in the water-soluble Au nanoparticles can be key materials for various biological sensing and detection systems.

Most recently, a successful procedure was reported to create various core−shell structures utilizing a redox-transmetalation process in organic media. Lee et al.[32−34] prepared a variety of core−shell structured nanoparticles with a cobalt core. Compared to conventional sequential reduction strategies, this transmetalation process has several advantages for the fabrication of core−shell structured nanoparticles: (1) no additional reducing agent is needed, (2) spontaneous formation of the shells deposited on the surface of the initial cores, (3) self-nucleation of secondarily added metals can be avoided, (4) inhomogeneous growth of the shells on the surface of the initial cores can be prevented.

In this work, the core/shell Ni/Au nanoparticles were chemically synthesized through a redox-transmetalation method in the reverse microemulsion solution. The method is a combination of the reverse microemulsion technique and the redox-transmetalation process, which can make the best of the two methods. To the best of our knowledge, this kind of synthesis method has not been reported. Because the approach did not need additional reagent to reduce the gold to form shells, just three kinds of microemulsion are enough to get a satisfied result. So, the influencing factor can be reduced, the microemulsion can be more stable, the synthesis of nanoparticles can be controlled more easily, and the expectation to get a better product can be ensured.

The chemical composition of the nanoparticles was determined by an inductively coupled plasma mass spectrometer. The structure and diameter of the resultant nanoparticles were characterized by X-ray diffraction (XRD), UV−visible absorption spectra, transmission electron microscopy (TEM), high-resolution transmission electron microscope (HRTEM), and Z-contrast image. The magnetic properties of the nickel nanoparticles were examined by the superconducting quantum interference device magnetometer.

Experimental Section

The nonionic surfactant polyoxyethylene lauryl ether (Brij30) was obtained from Arcos Chemical. *n*-Octane, nickel chloride, aurichlorohydric acid, sodium borohydride, acetone, and ethanol were supplied by GuangFu Chemical Reagent Factory. All the reagents were of analytical degree and used without further purification. The deionized water was degassed by bubbling argon through the water for 6 h. All solvents were degassed by the freeze−pump−thaw method and kept under argon protection before using.

The core−shell Ni−Au nanoparticles were chemically prepared through a redox-transmetalation method in reverse microemulsion. The reaction was carried out under argon protection at room temperature and stirred at a given speed. Brij30 and *n*-octane were used as the surfactant and the oil phase, respectively. The size of the water droplets in the reverse microemulsion constraining the growth of nanoparticles were controlled by the ω value (molar ratio of water to surfactant).

(17) Santra, S.; Zhang, P.; Wang, K. M.; Tapec, R.; Tan, W. H. *Anal. Chem.* **2001**, *73*, 4988.
(18) Wilcoxon J. P.; Provencio P. P. *J. Phys. Chem. B* **1999**, *103*, 9809.
(19) Chen, D. H.; Wu, S. H. *Chem. Mater.* **2000**, *12*, 1354.
(20) Chen, F. X.; Xu, G. Q.; Hor, T. S. A. *Mater. Lett.* **2003**, *57*, 3282.
(21) Bol, A. A.; van, B. R.; Meijerink, A. *Chem. Mater.* **2002**, *14*, 1121.
(22) Bana Irena; Drofenik Miha; Makovec, Darko *J. Magn. Magn. Mater.* **2006**, *307*, 250.
(23) Feng Jian; Zhang Chaoping *J. Colloid Interface Sci.* **2006**, *293*, 414.
(24) Cho, S. J.; Shahin, A. M.; Long, G. J.; Davies, J. E.; Liu, K.; Grandjean, F.; Kauzlarich, S. M. *Chem. Mater.* **2006**, *18*, 960.
(25) Tartaj, Pedro; Serna Carlos, J. *J. Am. Chem. Soc.* **2003**, *125*, 15754.
(26) Chen, D. H.; Hsieh, C. H. *J. Mater. Chem.* **2002**, *12*, 2412.
(27) Legrand, J.; Taleb, A.; Gota, S.; Guittet, M. J.; Petit, C. *Langmuir* **2002**, *18*, 4131.
(28) Cho, S. J.; Idrobo, J. C.; Olamit, J.; Liu, K.; Browning, N. D.; Kauzlarich, S. M. *Chem. Mater.* **2005**, *17*, 3181.
(29) Carpenter, E. E.; Seip, C. T.; O'Connor, C. J. *J. Appl. Phys.* **1999**, *85*, 5184.
(30) Zhou, W. L.; Carpenter, E. E.; Lin, J.; Kumbhar, A.; Sims, J.; O'Connor, C. J. *Eur. Phys. J. D* **2001**, *16*, 289.
(31) Lin, J.; Zhou, W. L.; Kumbhar, A.; Wiemann, J.; Fang, J. Y.; Carpenter, E. E.; O'Connor, C. J. *J. Solid State Chem.* **2001**, *159*, 26.
(32) Lee, W. R.; Kim, M. G.; Choi, J. R.; Park, J. I.; Ko, S. J.; Oh, S. J.; Cheon, J. *J. Am. Chem. Soc.* **2005**, *127*, 16090.
(33) Park, J. I.; Kim, M. G.; Jun, Y. W.; Lee, J. S.; Lee, W. R.; Cheon, J. *J. Am. Chem. Soc.* **2004**, *126*, 9072.
(34) Park, J. I.; Cheon, J. *J. Am. Chem. Soc.* **2001**, *123*, 5743.

The Ni cores were prepared by the reduction of Ni^{2+} with $NaBH_4$, and the ω value of 7 was selected to prepare the initial Ni nanoparticles. To begin with, 3 mL of a $NiCl_2$ (0.5 M) aqueous solution was added to 36 mL mixture composed of 9 mL of brij30 and 27 mL of *n*-octane to form the first reverse microemulsion solution, and the second reverse microemulsion solution containing 1 mL of $NaBH_4$ (3 M) with proportions identical to those in the first one was then added in drops. The solution immediately turned black upon the emergence of nickel nanoparticles. To ensure the thorough reduction of $NiCl_2$, we designed the mole ratio of $NaBH_4$ to $NiCl_2$ to be 2 and kept the reaction solution under argon protection for 12 h. In addition, 12 h was enough to ensure the spontaneous decomposition of excess $NaBH_4$,[35] because if it remained in the solution, the sequential redox-transmetalation reaction would be disturbed.

The gold shells formed on these Ni cores are driven by an in situ redox-transmetalation reaction between the Ni atoms on the surface of the Ni nanoparticles and $AuCl_4^-$ ion without any additional reducing agent. When $AuCl_4^-$ ions in a positive metal oxidation state approach the surface of Ni nanoparticles, which constitute the core structure, $AuCl_4^-$ ions can be directly reduced to gold through the sacrificial oxidation of the nulvalent nickel atoms and simultaneously deposited on the surface of Ni cores. Meanwhile, the Ni atoms are oxidized to Ni^{2+} and the electron transfer between the two metals results in core−shell type nanoparticles. Because this redox reaction can spontaneously proceed under favorable redox potential between the two metals, this method has been regarded as an efficient route for the selective formation of bimetallic structures.[36]

The reaction mechanism of the redox-transmetalation process can be expressed as

$$3Ni + 2AuCl_4^- \rightarrow 3Ni^{2+} + 2Au + 8Cl^- \quad (1)$$

The detailed procedures to synthesize the gold shells were presented as follows. The reverse microemulsion solution (11 mL) containing 1.5 mL of $HAuCl_4$ (0.5 M) was added to the solution of the initial Ni nanoparticles in drops at a slow speed. The ω value of $HAuCl_4$ solution was kept at 7 without any change. In other reported articles using a sequential reducing method, the ω value was increased to expand the water droplets within the reaction in order to accommodate the gold shell.[29] However, the ω value in present work was keep constant throughout the preparation process in order to maintain the droplet size and total droplet numbers in the solution, which could guarantee the formation of uniform gold shells. The mole ratio of Ni to Au was kept at 2 to ensure the formation of gold shell with proper thickness but keep from overeroding the initial Ni nanoparticles. The solution was kept under argon protection for another 12 h to ensure the completeness of redox-transmetalation process. The resultant core−shell Ni−Au nanoparticles in the solution were precipitated by centrifugation with the addition of ethanol, and then washed twice with the mixture of ethanol and acetone to remove the surfactants and other impurities. Finally, the nanoparticles were dried in vacuum at room temperature for 12 h.

The chemical composition of the nanoparticles was determined by a Varian Vista MPX inductively coupled plasma mass spectrometer (ICP-MS). The samples were first dissolved in aqua regia and then diluted to concentrations within the detection range of the instrument. X-ray diffraction (XRD) measurements were taken on a Rigaku D/max diffractometer with Cu Ka radiation at a wavelength of 1.5406 Å, and a step size of 0.02° to characterize

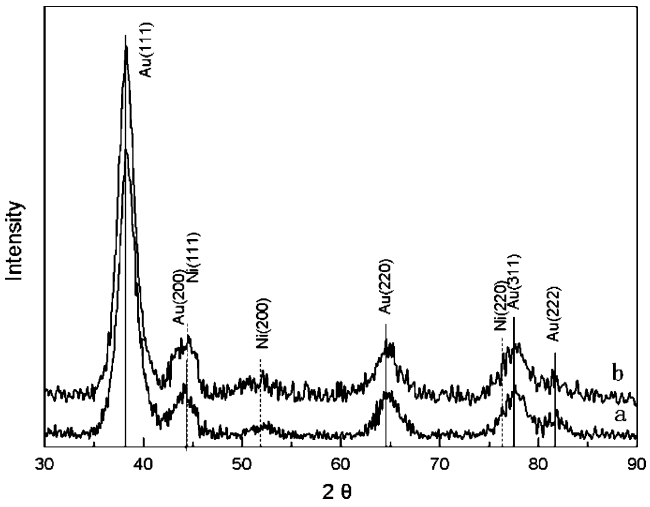

Figure 1. Powder XRD patterns of the core−shell Ni−Au nanoparticles obtained with Cu Kα radiation: (a) 1 day after synthesis, (b) exposed in air for 1 week after synthesis. The peak positions are referenced from PDF-2 Data Base. PDF 04-0784(Au) and 04-0850(Ni) are marked with solid and doted lines, respectively.

the structure of the core−shell Ni−Au nanoparticles. JADE5 software was utilized for data analysis. The crystallite size of nanoparticles is calculated by the Scherrer equation

$$L = 0.89\lambda/\beta(\theta)\cos\theta \quad (2)$$

where λ is the X-ray wavelength in nm, β is the intrinsic peak width in radians on a 2θ scale, θ is the Bragg diffraction angle, and 0.89 is the Scherrer constant. The morphology, dimension, lattice distances, and crystallographic structures of nanoparticles were studied by TEM, HRTEM, and Z-contrast image performed on a FEI Tecnai G2 F20 transmission electron microscope equipped with a high-angle annular dark field STEM detector. The sample for the TEM observation was prepared by dipping a copper-grid-supported transparent carbon foil in an ethanol solution in which the core−shell Ni−Au nanoparticles were suspended by sonication, and the grid was dried in open air. Energy-dispersive X-ray (EDX) spectroscopy attached to the TEM was also performed. UV−visible absorption spectra of colloid form samples with sizes similar to those of pure nickel, pure gold, and core−shell Ni−Au nanoparticles were obtained with a Shimadzu UV-365 spectrophotometer. A quantum design superconducting quantum Interference device (SQUID) PPMS-9 was used to measure the temperature and field dependence of the magnetization. Approximately 10 mg of sample was pressed and packaged in Teflon film and placed in a sample holder, measured by a vibrating sample magnetometer with a liquid helium continuous flow cryostat.

Results and Discussions

Elemental Analysis. The chemical compositions obtained from ICP analysis revealed that the proportion of nickel in weight was 14.3%, which approximately equals the expected value of 13.0%. Because a little portion of $HAuCl_4$ might not be reduced to gold and sequentially be washed away, the measured value was a little higher than the designed value.

X-ray Diffraction. Powder X-ray diffraction patterns of the synthesized core−shell Ni−Au nanoparticles are shown in Figure 1. The patterns indicate the presence of the crystalline gold with face-centered cubic (FCC) structure. The diffractions of the crystalline nickel are not as distinct

(35) Kreevoy, M. M.; Jacobson, R. W. *Ventron Alembic* **1979**, *15*, 2.
(36) Bosnich, B. *Inorg. Chem.* **1999**, *38*, 2554.

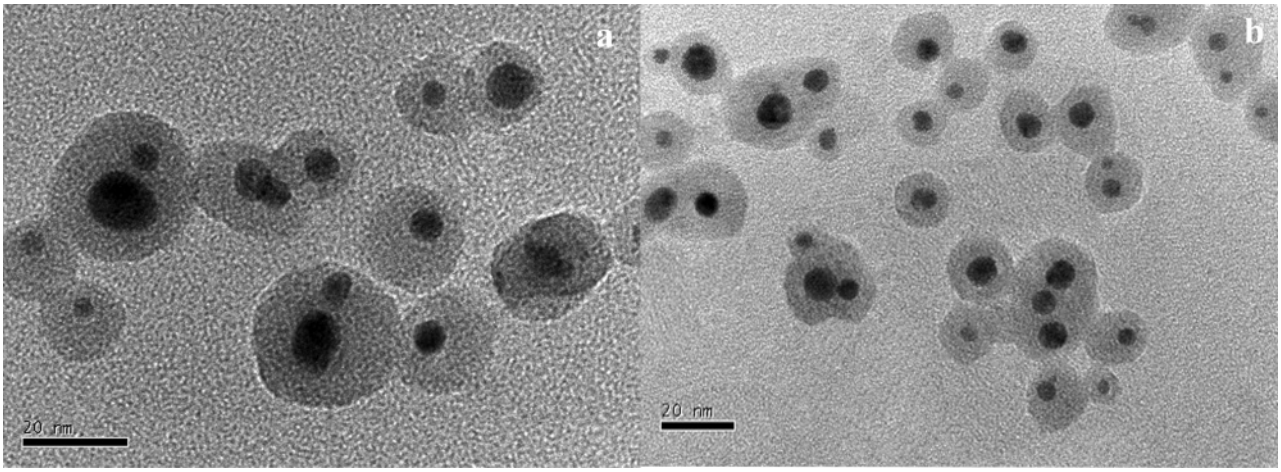

Figure 2. TEM micrograph of core−shell Ni−Au nanoparticles (a) 1 day and (b) 1 week after synthesis.

as those of gold because of the peak overlapping by gold. Three characteristic peaks of FCC structured nickel (2θ equal to 44.5, 51.8, and 76.4) corresponding with plane (111), (200), and (220) can be clearly seen. No other crystalline phases can be observed in the diffraction patterns. It can also be noticed that all peaks of the diffraction patterns are broad, which implies the particles have a very small size.

The diffraction patterns of the nanoparticles (in powder form) exposed in air for 1 week were similar to the patterns measured 1 day after synthesis, and no new diffraction peaks could be detected. Some possible oxides or hydroxides such as NiO, Ni_2O_3, or $Ni(OH)_2$ were not observed. The results indicated that no nickel oxides formed even after the nanoparticles were synthesized for a week.

The average crystallite size of the gold shells was about 8 nm by calculating with the Scherrer equation from the (111) Au diffraction, which well-accorded with the thickness of the gold shells.

Transmission Electron Micrographs. The core−shell structure of the nanoparticles is confirmed by the transmission electron micrograph, as shown in Figure 2.

From the TEM micrographs, the Ni cores and the gold shells can be clearly observed. The cores of the nanoparticles are estimated to range from 5−10 nm in diameter, the thickness of the shells are 5−10 nm, and the diameter of the integrated nanoparticles are estimated to range from 15 to 30 nm.

Some coalescence of the nanoparticles could be observed from the TEM images. This phenomenon may be due to the intensity of the interface formed by the surfactants not being strong enough to sustain the nanoparticles in the droplets. Some nanoparticles may get away from one water droplet, and then come into another one. So a water droplet may contain more than one Ni nanoparticle. When the $HAuCl_4$ was added to the synthesis of the gold shells, nanoparticles with more than one core would inevitably form. In subsequent research work, the interface will be strengthened by adjusting the composition of the solution.

After the nanoparticles deposited on the copper grid were exposed in the open air for 1 week at room temperature, the transmission electron micrograph (Figure 2 b) was similar to that one of the nanoparticles exposed for 1 day after synthesis (Figure 2a). The similarity of the above two images indicated that the core−shell structure had no change.

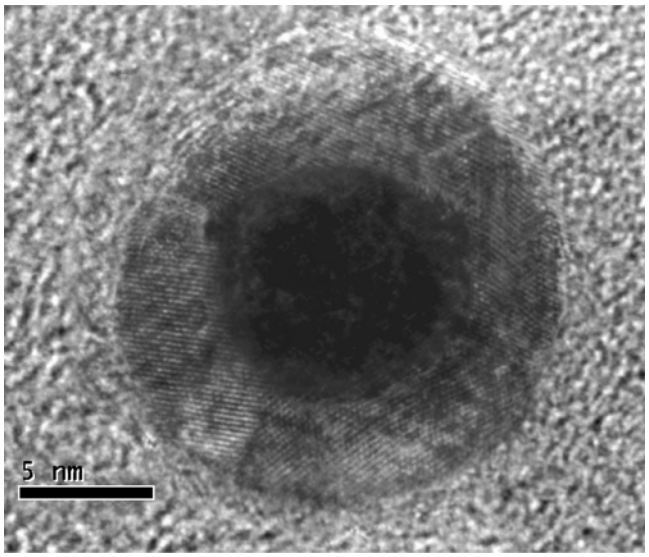

Figure 3. High-resolution TEM image of core−shell Ni−Au nanoparticles.

By focusing the EDX probe on the Ni cores of the nanoparticles prepared 1 day after synthesis, very weak peaks of oxygen were observed. The weight percentage of oxygen was round about 0.5%, which might result from the fractional NiO formed during the synthesis process because of the inevitable oxygen dissolved in the solvent, deionized water, and argon. For comparison, a sample exposed in the open air for 1 week was also analyzed. It was found that the peaks of oxygen hardly changed, proving that the nanoparticles were air-stable and that the oxidization process of the Ni cores hardly occurred. The Au proportion of the shell was much higher than that of the Ni core, implying that the shells were indeed formed by gold. In addition, boron was not detected, indicating that boron and boride were not left in the final products.

High-Resolution TEM. The gold shell of the synthesized core−shell Ni−Au nanoparticles is verified by the lattice patterns as shown in Figure 3.

According to the HRTEM image, well-developed lattice patterns can be clearly recognized in the shell of the nanoparticle. The lattice distance of 2.35 and 2.04 Å

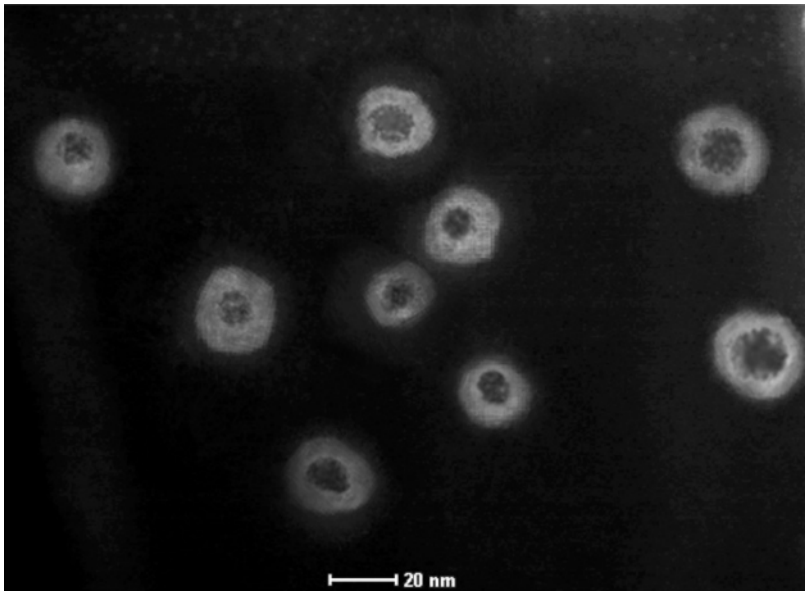

Figure 4. Z-contrast image of core−shell Ni−Au nanoparticles.

measured from the image are consistent with the lattice parameters of fcc (111) and (200) Au planes, respectively. In addition, the different crystallographic orientations of the gold shell indicate that the Ni core is surrounded by polycrystalline gold. This structure suggests that the gold has multiple nucleation sites on the surface of Ni core during the growth process of the shell. However, the lattice pattern of the core is not well-resolved because of its being both in a different crystallographic orientation and embedded inside the gold shell.

Because the crystallite size of the gold shells calculated from the (111) Au diffraction derived from the result of XRD is the average diameter of monocrystal in the gold shell, whereas the diameter of the gold shells obtained from TEM images is the diameter of the integrated nanoparticle, the difference in size is normally inevitable. Generally, the average crystallite size derived from XRD is smaller than the diameter of the gold shells obtained from the TEM images. In this circumstance, the smaller size derived from XRD, compared with the size obtained from TEM, should be ascribed to the presence of polycrystalline gold.

Z-Contrast Image. A Z-contrast image performed on these core−shell nanoparticles is shown in Figure 4.

In Z-contrast analysis, a high-intensity electron probe, typically subnanometer in diameter that determines the spatial resolution, is scanned across the sample and electrons incoherently scattered at high angles are detected by a high-angle annular detector. As the intensity of the scattered electrons is proportional to the square of the atomic number of the probed element, the element with higher atomic number will appear much brighter.

Z-contrast image of the core−shell Ni−Au nanoparticles shows the contrast difference between the relatively darker centers (lower atomic number) and the relatively lighter shells (higher atomic number), indicating the expected formation of Ni cores and gold shells.

UV−Visible Spectra. A series of UV−visible absorption spectra consisting of core−shell Ni−Au, pure Ni, and pure gold nanoparticles is shown in Figure 5.

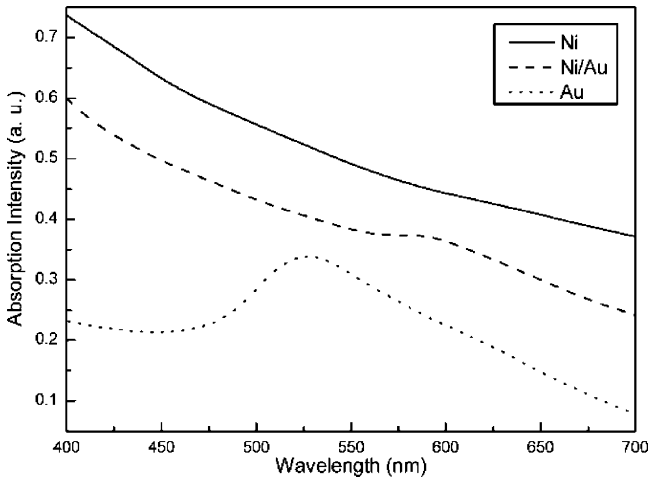

Figure 5. UV−visible absorption spectra of the core−shell Ni−Au, pure Ni, and pure gold nanoparticles with a similar diameter.

The absorption spectrum of the colloid-forming core−shell Ni−Au nanoparticles was measured and compared with that of the pure Ni and pure gold nanoparticle colloid prepared by the same way as shown in Figure 5. The gold colloid exhibits a distinct absorption band with a maximum around 530 nm; the spectrum of pure Ni cores is featureless with a monotonic decrease in absorbance with the increase in wavelength, whereas the core−shell Ni−Au nanoparticles colloid shows an absorption band with a maximum at 590 nm.

The absorbance of core−shell Ni−Au nanoparticles colloid shifting to higher wavelength compared to pure Au nanoparticles can be observed. This red shift behavior of the core−shell nanoparticles is attributed to the enhanced surface plasmon resonance absorption. The red shift in wavelength of gold surface plasmon has also been observed experimentally in other bimetallic systems with a metal core as well, such as core−shell Fe−Au and Co−Au nanoparticles.[30,14]

Magnetic Properties. Nickel is an important magnetic material. To investigate the magnetic properties of the core−

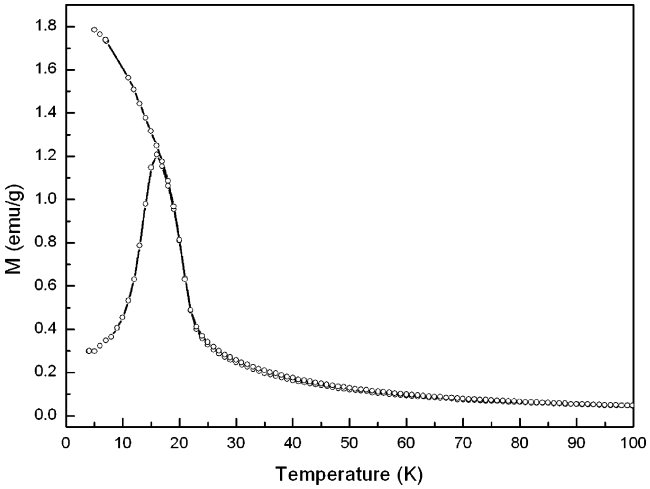

Figure 6. Temperature dependence of the magnetization of the core−shell Ni−Au nanoparticles, ZFC and FC curves, measured in a 100 Oe applied magnetic field.

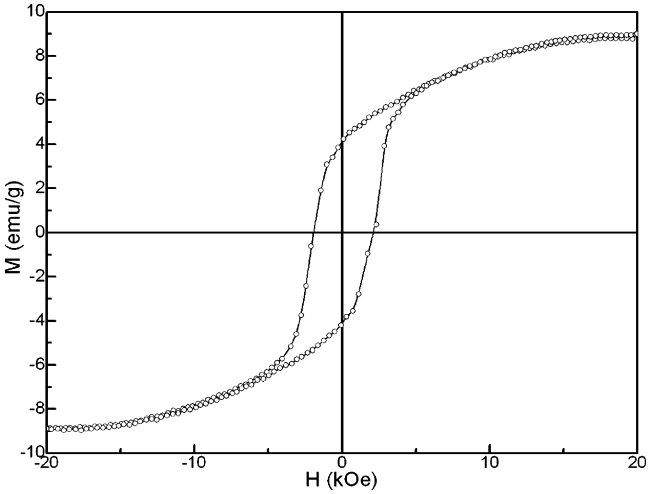

Figure 7. First-order reversal curves obtained at 5 K, normalized to the mass of Ni cores in the Ni−Au nanoparticles.

shell Ni−Au nanoparticles, we performed a series of magnetic measurements.

The zero-field-cooled (ZFC) and field-cooled (FC) temperature dependence of the magnetization were measured in a 100 Oe applied field, from 4 to 100 K, as presented in Figure 6.

For single-domain particles, the temperature of the maximum in the ZFC curve is regarded as the average blocking temperature (T_B), below which the sample is ferromagnetic and above which is superparamagnetic. The sharp maximum at 16 K in the ZFC curve indicates a clear blocking behavior of the sample. Accordingly, the T_B of the sample is 16 K. The overlap of the ZFC curve and the FC curve when the temperature was higher than T_B and the distinct deviation of the two curves at T_B indicates that the size of Ni cores in the nanoparticles have a narrow size distribution and the gold shells are thick enough to restrain the dipolar and transfer interactions among the Ni cores of different nanoparticles.

Because the nanoparticles are approximate independent single-domain nanoparticles and the interaction among the nanoparticles can be neglected, the thermally assisted magnetization reversal process can be described by

$$1/\tau = f_0 \exp(-K_a V/k_B T_B) \quad (3)$$

where τ of 30 s is a given measurement time, f_0, is frequency factor (1×10^9 s^{-1}), K_a is the magnetic anisotropy constant, V is the average volume of magnetic Ni cores, and k_B is Boltzmann constant.[37] So, K_a can be given by

$$K_a = \log(\tau f_0)(K_B T_B/V) \quad (4)$$

It is well-known that the superparamagnetic blocking temperature decreases with decreasing size of nanoparticles. For 7.5 nm diameter magnetic nanoparticles (the average diameter of the Ni cores synthesized in this work) with $T_B = 16$ K, $K_a = 10.48 \times 10^3$ J/m^3. For nickel with weakly anisotropic, a value of 5×10^3 J/m^3 is reported for bulk metal.[38] The high value of the anisotropy constant compared to the bulk is probably due to the very small size of the metal nickel domain in the particle. This could drastically increase the surface effect on the magnetic properties.

The magnetization curves, along with the hysteresis loops, of the core−shell Ni−Au nanoparticles were performed at 5 K, with the magnetic field cycle between −20 and +20 kOe. The magnetization curves are shown in Figure 7.

The hysteresis loop shown in Figure 4 indicates that the ferromagnetic behavior of the Ni−Au nanoparticles. Because the gold shells of the Ni−Au nanoparticles is paramagnetic and the proportion of gold is much higher than that of nickel, the magnetization was not saturated even when the applied magnetic filed reached 20 kOe. An attempt to separate the ferromagnetic and paramagnetic components from the original magnetization curves had been made by extrapolating the total magnetization of the nanoparticles in the high-field region (few thousand oersteds) as $M = M_s + xH$, where M_s is the saturation magnetization, x is the paramagnetic susceptibility. Through correcting the composition of the nanoparticles, 14.3 wt % of Ni as determined from ICP analysis, the M_s, remanent magnetization (M_r) and coercivities (Hc) of the nanoparticles were 9.0 emu/g, 4.1 emu/g, and 2 kOe, respectively.

The magnetization curves measured at 300 K are shown in Figure 8. It can be seen that no coercivity or remanence existed, indicating the superparamagnetic behavior of the sample. For nanoparticles below the critical size, superparamagnetic behavior can be shown at room temperature beause of the higher thermal fluctuation energy compared with anisotropic energy.[39] Adopting the extrapolating method mentioned above, the M_s of the Ni cores can be clearly determined as 0.7 emu/g, dramatically different form the M_s of 55 emu/g[38] at 300 K for bulk nickel metal.

The reduction in moment was due to the small size effect of the Ni cores, the accompanied increase in specific surface of the nanoparticles, and the oxidation of the Ni cores and the crystal lattice defects, etc. According to the Néel−Arrhenius equation, the magnetic saturation decreases with

(37) Cullity, B. D. *Introduction to Magnetic Materials;* Addison-Wesley: Reading, MA, 1972.

(38) Mutlu, R. H.; Aydinuraz, A. *J. Magn. Magn. Mater.* **1987**, *68*, 328.

(39) Himpsel, F. J.; Ortega, J. E.; Mankey, G. J.; Willis, R. F. *Adv. Phys.* **1998**, *47*, 511.

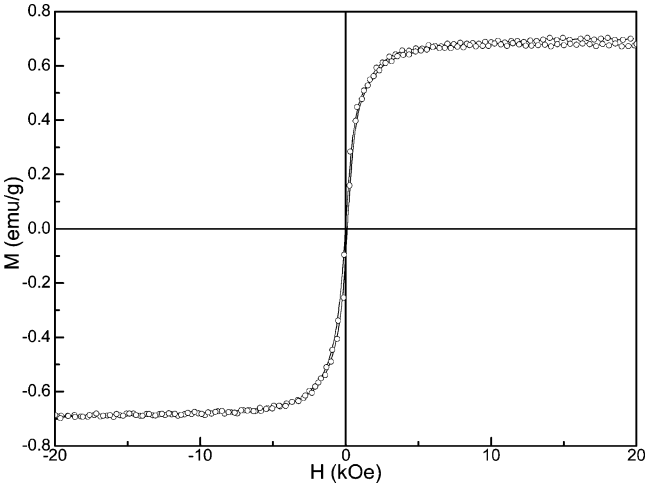

Figure 8. Magnetization curves obtained at 300 K, normalized to the mass of Ni cores in the Ni−Au nanoparticles.

the dimension of the magnetic particle reducing. The energy of a magnetic particle in an external field is proportional to its size or volume via the number of magnetic molecules in a single magnetic domain. When this energy becomes comparable to thermal energy, thermal fluctuations will significantly reduce the total magnetic moment at a given field.[40] In addition, the disorder structure of nickel at the interface between the Ni cores and the gold shells will result in nonmagnetic or weakly magnetic interfaces. It has been shown to cause a decrease in the effective magnetic moment.[41] Furthermore, the fact that the nickel at the interface lacks complete coordination and spins are likewise disordered is another important factor because of nickel's high specific surface.[40,42−44] Although the nickel nanoparticles had been washed before the magnetic measurement was performed, a very slight amount of the adsorbed surfactant on the nanoparticles could also cause a decrease in M_S. Accordingly, it is reasonable that the magnetic properties of nanoparticles are usually much smaller than that of the corresponding bulk materials.

Cho et al.[24,28] found that the Fe−Au nanoparticles they synthesized were gradually oxidized over time, indicating that the gold shell of the Fe−Au nanoparticles did not effectively protect the iron core from oxidation. They speculated that the oxygen can permeate into the shell because of the incomplete coverage and cracks in the gold shell. In our opinions, the possible reason of oxidization was that the $HAuCl_4$ reverse microemulsion solution was added before the second $NaBH_4$ reverse microemulsion solution. As a result, a portion of fresh Fe prepared in the former reaction procedure was oxidized to Fe^{2+} cation because of the strong oxidization effect of $AuCl_4^-$. The reaction could be expressed as follows

$$3Fe + 2AuCl_4^- \rightarrow 3Fe^{2+} + 2Au + 8Cl^- \qquad (5)$$

Then, the blended Fe^{2+} and $AuCl_4^-$ was reduced together by the sequential added $NaBH_4$ reverse microemulsion solution, so that Au shells blended with Fe would form instead of the anticipated pure gold shells. Once the particles synthesized by this approach were exposed to open air, the Fe in the shells would be oxidized to ferric oxide first so that the pores and cracks would form in the gold shells. The oxygen would then inevitably penetrate into the gold shell though those flaw to further oxidize the Fe core. Finally, the entire Fe core would be thoroughly oxidized.

In the present work, the synthesis approach has resolved the mentioned problem effectively. Because the gold shells were the result of $HAuCl_4$ directly reduced by the nickel cores, the $AuCl_4^-$ anion and Fe^{2+} cation could not be reduced at the same time. Accordingly, the flaws in gold shells could be greatly diminished and the nanoparticles could more effectively resist the oxidization effect in open air.

Conclusions

The core−shell Ni−Au nanoparticles were prepared using the redox-transmetalation method in reverse microemulsion. Elemental analysis verified that the nanoparticles are composed of Ni and Au, and boron and boride were not left in the final results. The powder XRD patterns revealed the presence of FCC structured crystalline gold and nickel and the absence of any crystalline nickel oxides, nickel boride, or other crystalline byproducts. The structure of the Ni core and gold shell of nanoparticles is confirmed by HRTEM, Z-contrast, and UV−visible absorption spectra. Comparing the EDS results of 1 day with that of 1 week confirms that the percentage of oxygen is almost same. The gold shells coated on the Ni cores can effectively relieve the oxidization process of the Ni cores. The T_B of the nanoparticles equals to 16 K. Below T_B, the nanoparticles were ferromagnet. Above T_B, no coercivity or remanence was observed, and the typical superparamagnetic behavior was presented at 300 K. The core−shell Ni−Au nanoparticles with inert gold coatings presented here show a great promise as nickel-based nanoparticles.

Acknowledgment. The authors acknowledge the financial support by the Specialized Research Fund for the Doctoral Program of Higher Education, China (20050056041).

CM070182X

(40) Shafi, K. V. P. M.; Gedanken, A.; Prozorov, R.; Balogh, J. *Chem. Mater.* **1998**, *10*, 3445.
(41) Hwang, J. H.; Dravid, V. P.; Teng, M. H.; Host, J. J.; Elliott, B. R.; Johnson, D. L.; Mason, T. O. *J. Mater. Res.* **1997**, *12*, 1076.
(42) Lin, Z.; Cai, J. J.; Scriven, L. E.; Davis, H. T. *J. Phys. Chem.* **1994**, *98*, 5984.
(43) Kodama, R. H. *J. Magn. Magn. Mater.* **1999**, *200*, 359.
(44) Sato, T.; Iijima, T.; Seki, M.; Inagaki, N. *J. Magn. Magn. Mater.* **1987**, *65*, 252.